Journal of Power Sources 196 (2011) 4044–4053

Contents lists available at ScienceDirect

Journal of Power Sources

journal homepage: www.elsevier.com/locate/jpowsour

Tailoring of RuO_2 nanoparticles by microwave assisted "Instant method" for energy storage applications

Abirami Devadas, Stève Baranton*, Teko W. Napporn, Christophe Coutanceau

Laboratoire de Catalyse en Chimie Organique (LACCO), Equipe Electrocatalyse, UMR 6503 CNRS-Université de Poitiers, 40 avenue du Recteur Pineau, 86022 Poitiers Cedex, France

ARTICLE INFO

Article history:
Received 3 September 2010
Received in revised form 3 November 2010
Accepted 27 November 2010
Available online 13 December 2010

Keywords:
RuO_2
Instant method
Microwave
In situ XRD
OER
Supercapacitor

ABSTRACT

RuO_2 nanoparticles are synthesized by Instant method using Li_2CO_3 as stabilizing agent, under microwave irradiation at 60 °C and investigated for the anodic oxygen evolution reaction (OER) and for their supercapacitance properties in 0.5 M H_2SO_4 medium. Structural and morphological characterizations of RuO_2 are investigated by *in situ* X-ray diffraction (XRD), thermogravimetric analysis (TG-DTA), transmission electron microscopy (TEM), energy dispersive X-ray analysis (EDS) and Raman spectroscopy. The TEM images of as prepared material show the uniform distribution of RuO_2 nanoparticles with mean diameter of ca. 1.5 nm. Analysis on as prepared material indicates the structural formula as $[RuO_2{\cdot}2.6H_2O]$ $0.7H_2O$ with low crystallinity. The influence of annealing temperature on RuO_2 is studied in light of electrocatalytic activity for oxygen evolution reaction (OER) and capacitance. Electrochemical performances of RuO_2 electrodes are followed by current–potential curves, galvanostatic charge–discharge cycles and evolved oxygen measurements. The amount of oxygen gas evolved during the OER by the crystalline RuO_2 is found to be consistent with the electrical energy supplied to the catalyst. The cyclic voltammogram of RuO_2 exhibits the typical capacitance behavior with highly reversible nature. The specific capacitance of hydrous RuO_2 is found to be 737 $F\,g^{-1}$ at the scan rate of 2 $mV\,s^{-1}$, by the balanced transport of proton through the structural water and electron transport along dioxo bridges, which makes a suitable material for energy storage. The specific capacitance decreases with increase in the crystallinity of RuO_2. The present study shows the potential method to synthesize rapid and uniform nano particles of RuO_2 for water electrolysis and supercapacitors.

1. Introduction

The search for new electrocatalysts, especially DSA-type anodes has been greatly responsible for the advances in electrocatalysis [1]. Great effort has been put into the development of new electrocatalysts capable of selectively catalyzing the four-electron reaction for water oxidation. Advanced water electrolysers using proton exchange membranes (PEM) are less common and generally utilize Pt, Ir, Ru, Au, Ag, Rh based materials. Oxygen evolution reaction (OER) occurs on noble metal electrodes and the oxides of noble metals are normally more active. Generally, the oxides are more stable than metals, especially when used as anode, as they cannot be further oxidized easily. Basic studies on the surface structure-electrochemical reactivity relationship of conducting metal oxides have been carried out due to their wide importance in electrochemistry. Due to high electrochemical performance, ruthenium oxide (RuO_2) and iridium oxide (IrO_2) have been extensively investigated as anodes for O_2 evolution in acidic medium [2–5].

RuO_2 exhibits interesting properties such as low resistivity, high chemical and thermodynamic stability under electrochemical environment. Non stoichoimetric RuO_x shows better catalytic performance by supplying the sites to adsorb the hydroxyl radicals from water. The well-known application of RuO_2 is as an electrode in energy storage electrochemical supercapacitors [6]. Among the many transition metal oxides, the most success has been achieved using RuO_2 for supercapacitors due to its advantages of a wide potential window of highly reversible redox reactions, long life cycle and metallic type conductivity [7]. In particular, RuO_2 has very high stability and low overpotentials for O_2 and Cl_2 production [8]. It may also be advantageous for H_2 production and not very susceptible to contamination by metal deposition or organic molecules [9].

Various methods for the synthesis of RuO_2 were developed, such as sol–gel method [10], polyol method [11], Adams fusion method [12], etc. The focus on RuO_2 thin films by MOCVD method [13], spray pyrolysis [14], spin coating [15], RF magnetron sputtering [16], pulse-laser deposition [17], colloidal method [18], etc. had also been described by many researchers. Despite of its extensive use in industry and its potential applications, the synthesis of the RuO_2 by a method giving high yield at the expense of less

* Corresponding author. Tel.: +33 5 49 36 64 14; fax: +33 5 49 45 35 80.
E-mail address: steve.baranton@univ-poitiers.fr (S. Baranton).

0378-7753/$ – see front matter © 2010 Elsevier B.V. All rights reserved.
doi:10.1016/j.jpowsour.2010.11.149

number of precursors in less duration needs to be probed. The microwave heating, which is rapid, easy and very energy efficient, has been used for a lot of applications over the two last decades [19]. Recent studies on the preparation of Ruthenium oxide-multi walled carbon nanotube (MWCNT) composites have been performed by microwave irradiation [20,21]. Significant enhancement in specific capacitance of RuO_2/MWCNT composites has been obtained via microwave method. A simple synthetic procedure called "Instant method" involving the basic hydrolysis of H_2PtCl_6 with Li_2CO_3 and different types of carbon support for the preparation of Pt nanoparticles was proposed and patented by Reetz et al. [22] and Reetz and Lopez [23]. This method is of great interest, because it is fast, especially without using an organic stabilizer and the synthesis takes place in water.

In the present study, a fundamental investigation on RuO_2 materials prepared by the "Instant method" assisted by microwave irradiation is explored. For this synthesis of RuO_2 nanoparticles, Li_2CO_3 is used as the stabilizing agent and treated under microwave irradiation at 60 °C. The prepared compounds are investigated for the OER and for supercapacitance applications in 0.5 M H_2SO_4 medium. The prepared RuO_2 compounds are characterized by *in situ* XRD, TG-DTA, TEM and Raman analysis. The effect of thermal treatment on the structure and performance of RuO_2 as catalyst for anodic oxygen evolution and as material for supercapacitance is explored. The RuO_2 nanoparticles prepared using microwave technique is expected to have better catalytic performance toward OER. A relationship between structure and electrochemical properties will then be proposed by measuring the specific capacitance and the amount of evolved oxygen for a specified time.

2. Experimental

2.1. Preparation of RuO_2 by Instant method

$RuCl_3{\cdot}xH_2O$ (Alfa, 99.9%) and Li_2CO_3 (Sigma–Aldrich, 99%) were employed as the precursors. The calculated amount of $RuCl_3{\cdot}xH_2O$ solution is added dropwise to 50 mL of solution containing Li_2CO_3, under stirring of 500 rpm. The final mixture was prepared to have 0.01 M $RuCl_3{\cdot}xH_2O$ and 0.04 M Li_2CO_3. The pH of the mixture was maintained between 9 and 10. The mixture was treated under microwave irradiation (oven MARS 5, CEM Corporation) with the power of 400 W for 20 min, by keeping the temperature at 60 °C. For comparison, the material was also prepared by classical heating route. Classical method involves heating the mixture to 60 °C for 6 h, with a temperature controlled hot plate with stirring under 500 rpm. The synthesized oxide nanoparticles were separated from solution by centrifugation (Sigma, 2-16PK) under 15,000 rpm at 30 °C. The product was washed using water–ethanol mixture, until free of chloride and then dried at 80 °C. The classical and microwave assisted synthesized materials were designated as R-C-80 and R-M-80, respectively. The R-M-80 was annealed at different temperatures in air with the ramp rate of 3 °C min^{-1}, namely, 200 °C, 350 °C and 600 °C for 1 h and referred hereafter as R-M-200, R-M-350 and R-M-600, respectively.

2.2. Physical and physicochemical characterizations

The thermogravimetric analysis (TGA) was carried out using a thermobalance Q600 DTA instrument. The measurements were done by heating the sample from 25 to 700 °C with a heating rate of 10 °C min^{-1} under the air flow of 100 mL min^{-1}. *In situ* X-ray diffraction (XRD) patterns were recorded on a X-ray diffractometer (Brucker, D 8 Advance) with copper target (K_α = 1.5405 Å) powered at 40 kV and 40 mA. The analysis was performed by heating the sample from room temperature up to 600 °C, with a ramp of 10 °C min^{-1} under air atmosphere. The measurements were carried out in the 2θ range of 10°–70° in step mode of 0.06° and a fixed acquisition time of 5 s $step^{-1}$. Raman spectra for the samples were recorded using a Raman confocal microscope HORIBA JOBIN YVON HR800 UV, attached with an internal laser He–Ne emitting with a wavelength of 632.81 nm and a CCD detector. Surface morphology was examined using transmission electron microscope (JEOL 2100, UHR, 200KV) and the qualitative analysis of the samples was made by EDS analyzer equipped with a LaB_6 filament. The mean particle size and size distribution were determined by measuring the diameter of 250 isolated particles using ImageJ free software.

2.3. Electrochemical measurements

The electrochemical measurements were carried out in a standard three electrode electrochemical cell. A glassy carbon plate was used as the counter electrode and the reversible hydrogen electrode (RHE) as reference electrode, which was connected through a luggin capillary to the working electrode compartment. A solution of 0.5 M H_2SO_4 (Merck, Suprapur) in ultrapure water (Milli-Q, Millipore, 18.2 MΩ cm) was used as the electrolyte. All the potentials were referred to that of the RHE. The polished glassy carbon as the working electrode with 0.071 cm^2 geometric surface area was used. The voltage–current density curves were recorded using a high power potentiostat (VoltaLab PGZ 402) connected with a computer, to apply current sequences as well as to store data. Anodes were prepared from the ink consisting of 10 mg of prepared material in 1 mL of H_2O + 0.1 mL of Nafion (5 wt% in aliphatic alcohol from Aldrich). For recording the polarization curves, the working electrode was prepared by depositing 5 μL of the ink on the polished glassy-carbon electrode (0.64 $mg_{catalyst}$ cm^{-2}) and the electrochemical measurement was recorded at fixed scan rate of 10 mV s^{-1}. Before each experiment, the electrolyte was purged by bubbling nitrogen (U quality) for 15 min and the nitrogen atmosphere was maintained in the electrochemical cell for the experiment.

2.4. O_2 evolution measurement

A conventional three-electrode electrochemical cell was equipped with gas recuperation on the top. An integrated apparatus is designed, to quantify gas-volumetric (GV) measurements in the reaction. The reactor is coupled to a self assembled spiral tube water reservoir and a collection chamber with a calibrated microbalance (accuracy of 0.1 mg). The volume of evolved O_2 during the reaction was quantified by water displacement through a spiral water reservoir connected to the cell. In particular, such equipment is useful to quantify the molecular oxygen produced in micro level. The working electrode was prepared by depositing 25 μL of the ink (0.2275 $mg_{catalyst}$) on the polished rectangular gold electrode of 1 × 0.5 cm^2 geometric surface area for this study.

2.5. Specific capacitance studies

In the three electrode electrochemical cell, the capacitive current density measurements were carried out with a glassy carbon plate as counter electrode and the RHE as reference electrode. For the specific capacitance measurement, 1.5 μL of an ink which contains 1 mL ultrapure water, 0.1 mL of Nafion solution 5 wt% in aliphatic alcohol and 10 mg of ruthenium oxide compound, was deposited on the polished 3 mm diameter glassy carbon electrode, yielding 0.0136 mg of the material. The cyclic voltammograms were recorded from 0.3 to 1.2 V vs. RHE at different scan rates in 0.5 M H_2SO_4 medium.

3. Results and discussion

3.1. Structural characterization

The as prepared catalyst (R-M-80) is characterized by *in situ* XRD, TEM, Raman and TG-DTA.

3.1.1. X-ray diffraction measurements

XRD pattern of R-M-80 is shown in Fig. 1. The absence of well defined diffraction peaks for R-M-80 implies that the formed RuO_2 is poorly crystalline. It can be assumed that the particle sizes of R-M-80 are very low, which might have escaped from X-ray diffraction. The structural change of R-M-80 with annealing temperature was followed using *in situ* X-ray diffraction and the corresponding diffractograms are depicted in Fig. 1. Thermal treatment of the R-M-80 up to 200 °C, did not lead to any drastic changes in XRD pattern (Fig. 1 inset). When the temperature is raised to 350 °C, sharp well defined peaks located at 28°, 35° and 54° corresponding to crystalline RuO_2 (1 1 0), (1 0 1) and (2 1 1) orientations are clearly observed, indicating long-range crystalline order. Earlier, it was observed that complete crystalline phase of ruthenium oxide is obtained at relatively high annealing temperatures (300 °C) [7]. It was also reported that by the electrostatic spray deposition (ESD) [24], the formation of crystalline phase RuO_2 thin film occurred at 200 °C. The diffractogram of RuO_2 material prepared by the "Instant method" have the prominent peak at 35° of (1 0 1) plane. However, based on the broadness of XRD peak at 35°, the crystallite size (D) has been calculated using the Scherrer equation (1).

$$D = \frac{0.9\lambda}{\beta_{1/2} \cos \theta} \quad (1)$$

where λ is the wavelength (Å) of characteristic X-ray applied, $\beta_{1/2}$ is the line broadening at full width half the maximum intensity (FWHM) in radians.

The mean crystallite sizes obtained using Scherrer's formula as a function of calcination temperature are shown in Fig. 2. The calculated crystallite size is found to be approximately 1.4 nm for the sample R-M-80, which is in agreement with the particle size obtained from TEM measurements (Fig. 3A and B). When the sample is annealed to 200 °C, the crystallite size slightly increased to 1.7 nm. Further increase in temperature to 250 °C leads to substantial increase in the crystallite size which accounts to 14 nm. At 350 °C, it is found to be 19 nm. The aggregation of the nanoparticles occurred as most of the water molecules are lost before this temperature. It was reported that the absence of structural water may result in the coalescence and growth of ruthenium oxide nanoparticles to form larger crystals [25]. The crystals might have grown and its size is calculated to be 23 nm, when the annealed temperature increased up to 600 °C (Fig. 2).

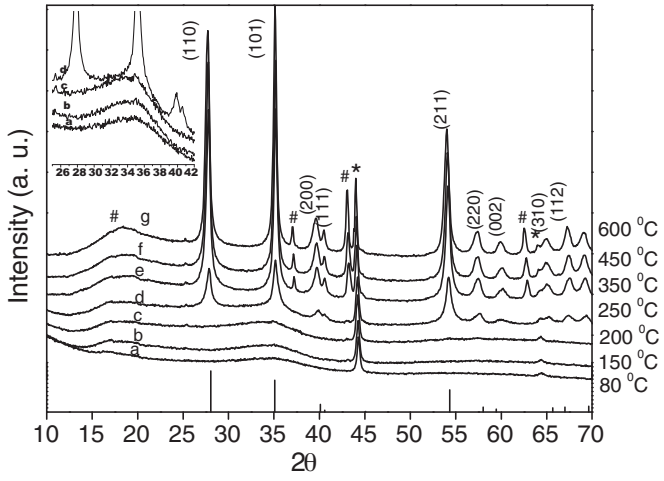

Fig. 1. *In situ* XRD pattern of R-M-80 sample upon annealing in air. *Sample holder; #Lithium ruthenium oxide; characteristic peaks of RuO_2 from JCPDS 88-322 are shown as lines.

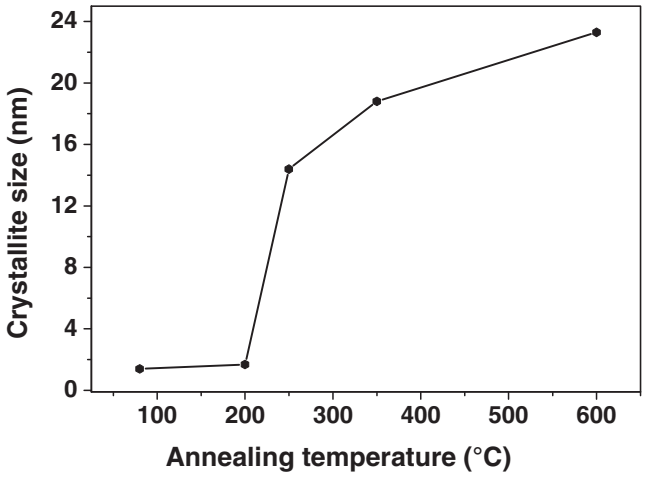

Fig. 2. Crystallite size calculated using Scherrer equation from XRD peak at 35° (2θ).

The presence of peaks corresponding to lithium ruthenium oxide (JCPDS 85-2001) can be observed in the diffractogram after annealing at 350 °C (Fig. 1). These peaks may be due to the lithium residue associated during the preparation of the ruthenium oxide compound (Section 2.1).

In order to check the possibility of formation of the RuO_2 crystalline phases at lower temperatures, *in situ* XRD patterns have also been measured under oxygen atmosphere. The results illustrated that there is no notable difference in the temperature for the formation of crystalline RuO_2 with the annealing atmospheres being either air/oxygen (not shown). Thus the distinct samples are chosen for further characterizations by annealing R-M-80 at different temperature and designated as R-M-200, R-M-350 and R-M-600 at 200 °C, 350 °C and 600 °C respectively.

3.1.2. TEM measurements

The homogeneous distribution of particle size is observed from TEM images of R-M-80 (Fig. 3A), which is clearly seen in the histogram (Fig. 3B). The average diameter of RuO_2 particles are in the order of 1.5 nm. EDS analysis reveals the atomic ratio of Ru/O is higher than 2 for R-M-80, which substantiates the formation of hydrous RuO_2 and is supported by thermogravimetric analyses. Moreover, HRTEM of R-M-80 clearly shows the partially crystalline nature of RuO_2 (Fig. 3C). The distance between the lattice fringes of R-M-80 is found to be 0.25 nm, which coincides with the distance calculated from the XRD peak position at 35° (Fig. 1). After a heat treatment at 200 °C (R-M-200) uniform RuO_2 nanoparticles remain as observed on Fig. 4A. The TEM image for the material R-M-350 shows the nanostructures of RuO_2 crystals in Fig. 4B. These RuO_2 nanostructures have the particle size varying between 7 nm and 18 nm. Due to the annealing temperature, the water molecules in hydrous form are removed and well defined crystals of RuO_2 are obtained, as shown in the HRTEM image of the R-M-350 (Fig. 4C). It is in agreement from the EDS analysis of R-M-350, that the atomic ratio of Ru/O is found to be around 2, which implies that the obtained oxide of Ruthenium is RuO_2. The TEM image of R-M-600 shows the aggregation of nanoparticles in Fig. 4D.

3.1.3. Raman spectroscopy

The Raman spectrum of the sample R-M-80 (Fig. 5) shows three major Raman features, namely the E_g, A_{1g} and B_{2g} modes, centred at

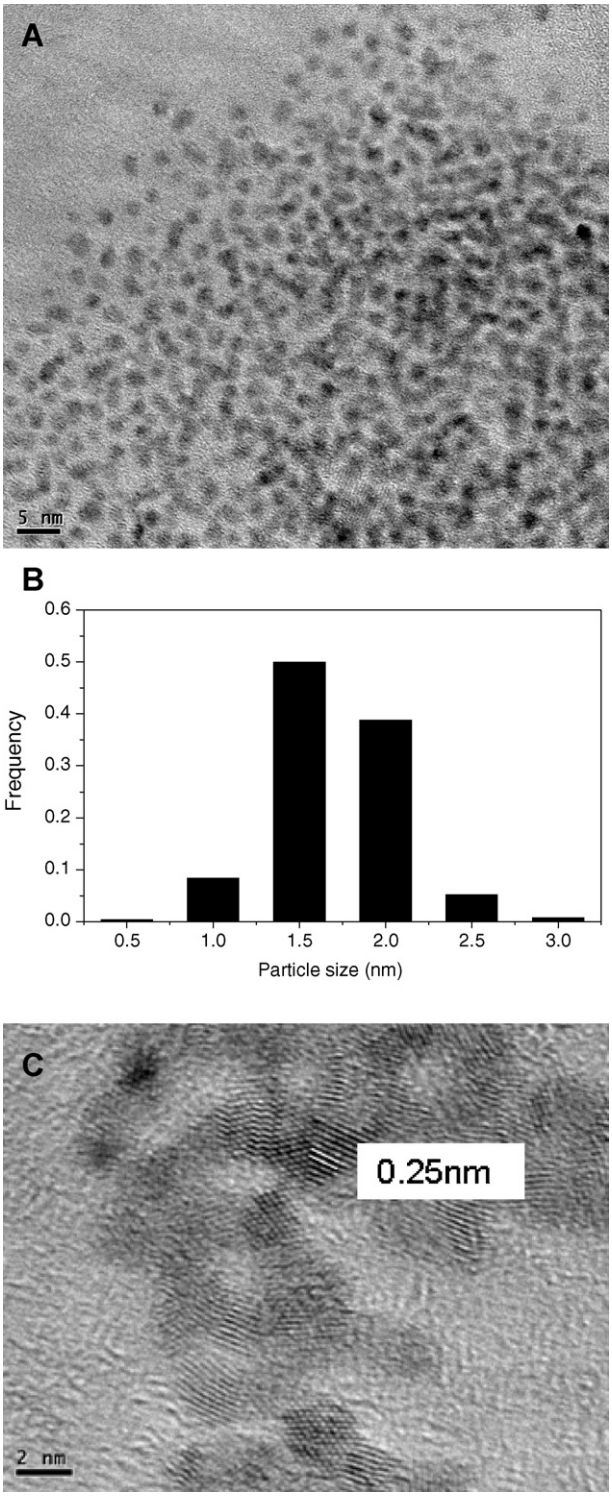

Fig. 3. (A) TEM images of R-M-80, (B) related histogram of particle size distribution and (C) HRTEM for R-M-80.

501 cm^{-1}, 619 cm^{-1} and 677 cm^{-1}, respectively. Based on Raman-active phonon frequencies predicted by group theory [26], the single crystal of Rutile type RuO_2 has the characteristic spectrum with four bands at 528 cm^{-1}, 646 cm^{-1} and 716 cm^{-1} for E_g, A_{1g} and B_{2g} modes, respectively. Generally, the Raman spectra of thin films are considerably different than those of the single crystal features. Due to the low annealing temperature, the extent of red shift in Raman spectra is found to be higher for R-M-80. This result clearly demonstrates the formation of poorly crystalline RuO_2 nanoparticles or small crystallites of RuO_2 in as prepared material (R-M-80) and the XRD measurement indicates a poor crystallinity of this sample.

Raman analysis for the annealed samples shows the peak sharpening and significant shift in the peak position. The Raman bands for the samples R-M-200 is observed at 504 cm^{-1}, 622 cm^{-1} and 682 cm^{-1}, whereas they are shifted to 507 cm^{-1}, 626 cm^{-1} and 688 cm^{-1} for R-M-350 (Fig. 5). As the particle sizes are increasing, the band positions in Raman spectra are also found to be shifted. This shift in the peak position can be associated with the change in crystallite sizes of RuO_2 (as observed from TEM images) and in the level of crystallinity of the material [26]. The shift in peak positions of these bands are closer to the characteristic bands reported for RuO_2 aerogels by Ryan et al. [27].

3.1.4. Thermogravimetric analysis

The TGA of R-M-80 shows a total weight loss of ca. 40 wt% when increasing the temperature from 25 °C to 700 °C (Fig. 6A). The weight loss is observed in three distinct temperature regions. The first weight loss with a broad endothermic peak around 60–70 °C, is assigned to the physically adsorbed water. A drastic weight loss (ca. 32 wt%) in the temperature range of 100–350 °C, occurred with an exothermic nature (Fig. 6A). This weight loss can be assigned to loss of structurally or chemically bounded water molecules [21]. There is a small weight loss (ca. 0.7 wt%) between 350 °C and 700 °C. Thus, the removal of structural water, in the temperature range from 100 °C to 700 °C, resulted in 35% of weight loss. This equals to 2.6 mol of water molecules per mole of RuO_2. The physically adsorbed water in the temperature range from 25 °C to 100 °C led to a weight loss of 7%, which corresponds to 0.69 mol of water per mole of hydrous RuO_2. From TGA, the structural formula of R-M-80 can be derived as $[RuO_2{\cdot}2.6H_2O]$ $0.7H_2O$. The TG analysis of R-M-200 (Fig. 6B) presented around 10% of total weight loss with 1.7% below 100 °C and 8.3% from 100 °C to 700 °C. The structural water is found to be 0.6 mol mol^{-1} of RuO_2. Thus it is derived that the R-M-200 (Fig. 2B) material has the structural formula as $[RuO_2, 0.6H_2O]$ $0.14H_2O$. Fig. 6C shows the TG analysis of R-M-350 and weight losses of 1% and 3.5% are observed for physisorbed and chemically bounded water molecules (structural water), respectively. Hence, structural water equals to 0.3 moles of water molecules per mole of RuO_2. Therefore the structural formula of R-M-350, is derived as $[RuO_2{\cdot}0.3H_2O]$ $0.08H_2O$ from TGA. It is interesting to note that about 0.3 mol of H_2O are present even after calcination of RuO_2 at 350 °C (in R-M-350). These values are comparable to the reported water molecules determined in RuO_2 [29]. For both R-M-200 and R-M-350 samples, the exothermic water loss reported for R-M-80 sample between 100 °C and 350 °C is also observed. Finally, around 1% of total weight loss is observed from R-M-600 (Fig. 6D) from which the structural formula can be determined as $[RuO_2{\cdot}0.05H_2O]$ $0.03H_2O$.

3.2. Electrochemical performance for OER

The current–potential curves for the oxygen evolution reaction are compared in Fig. 7 for the as prepared catalyst under microwave radiation (R-M-80) with the classically prepared catalyst (R-C-80). For R-M-80, the oxygen evolution begins around 1.4 V vs. RHE in 0.5 M H_2SO_4 medium. But at higher potentials, the catalyst becomes inactive, as observed with the decrease of the current density on the polarization curve. Similarly, R-C-80 presents an oxygen evolution almost at the same potential and becomes inactive at higher potentials, but R-M-80 catalyst allows reaching higher current density than R-C-80. In addition to higher current density, the microwave route was chosen to synthesize RuO_2 nanoparticles by Instant method due to a lower synthesis time and a better control

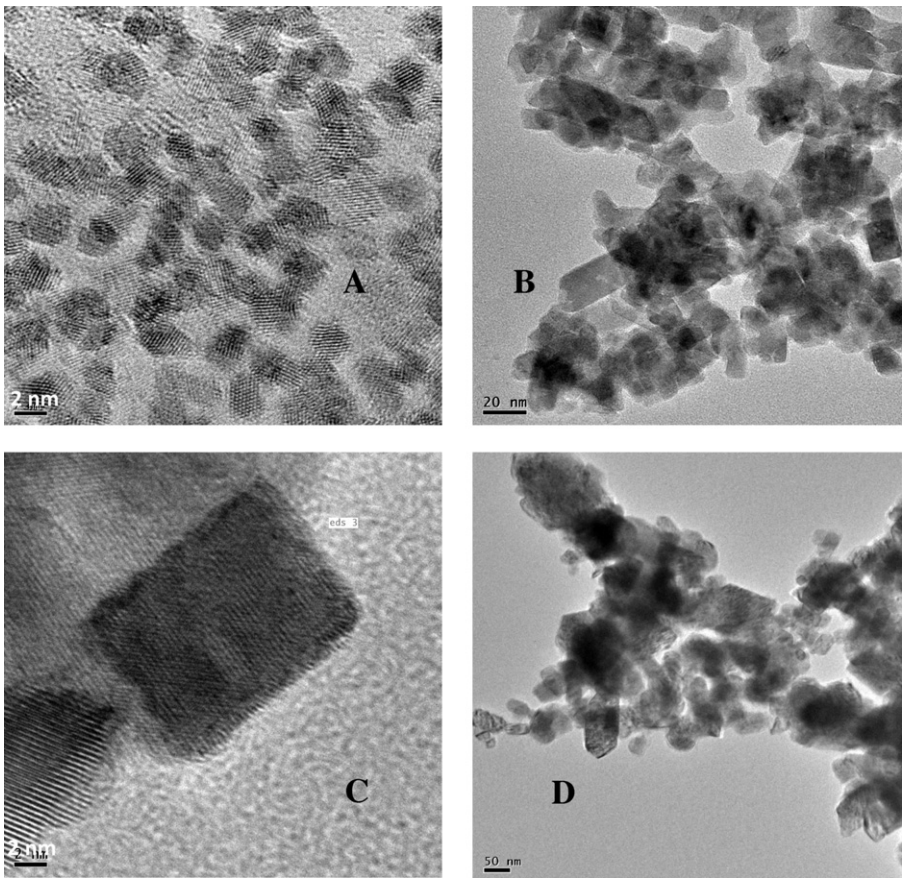

Fig. 4. (A) TEM image of R-M-200 sample, (B) TEM image of R-M-350 sample, (C) HRTEM image of R-M-350 sample, (D) TEM image of R-M-600 sample.

of the temperature resulting in uniform RuO_2 nanoparticles which could have led to the higher current density observed for the OER on R-M-80 than on R-C-80.

The electrochemical studies in acid medium have also been performed for the compounds annealed at different temperatures. The catalyst annealed at 200 °C (R-M-200) was chosen since the commencement of X-ray diffraction peaks is observed after 200 °C (Fig. 1). On the TEM image shown in Fig. 4A, R-M-200 is found to have a uniform nanoparticles size as found in R-M-80 sample with a slight increase in particle size. This may be due to the hydrous as well as poorly crystalline oxide, which is evidenced by *in situ* XRD (Fig. 1) and also slight increase in particle size is demonstrated by the shift in the peak position of the Raman spectra (Fig. 5). The catalyst R-M-200 is tested for OER and the oxygen evolution begins before 1.4 V vs. RHE with a large current density, but this current density decreases drastically at higher potentials (Fig. 8). The reason for the larger current and instability of the catalyst at higher potential may be related to the hydrous nature of the catalytic material. The annealing temperature of the catalyst is further increased to 350 °C, the obtained catalyst (R-M-350) demonstrated the anodic oxygen evolution with a more important current density and also current density is found to increase with increasing potential. When the ruthenium oxide compound is further annealed to 600 °C, the polarization curve for the oxygen evolution is not stable at higher potentials. The decrease in activity of the R-M-600 catalyst at high potentials may be related to the loss of water molecules which favor aggregation process of nanoparticles (Fig. 4D), leading to a decrease in the accessibility for the active surface sites of the catalyst. The crystallite growth process evidenced from XRD measurements (Fig. 2) may also participate to the decrease of the catalyst active surface area. This work confirms the influence of annealing temperature or crystallinity of RuO_2 on the anodic evolution of oxygen in acid medium. However, it is very difficult in the case of R-M-600 catalyst to explain the unstable behavior observed during OER (Fig. 8). The morphology, stability and electro-catalytic activity for oxygen evolution of the electrode material depends greatly on the preparation conditions [26], increasing the electroactive surface area and accessibility to active sites [28,29].

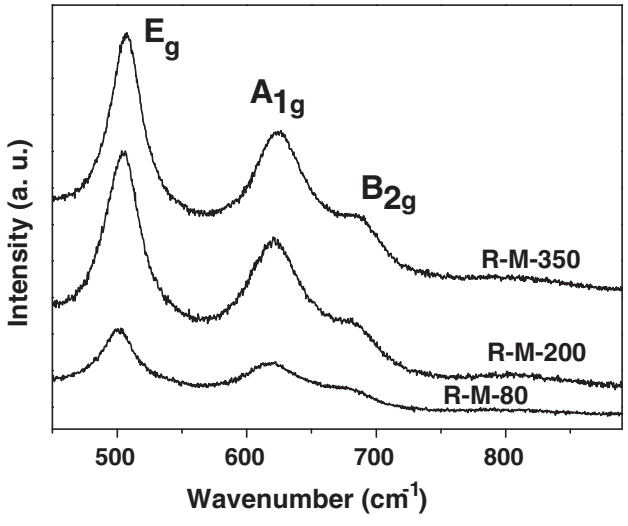

Fig. 5. Raman spectra of the ruthenium oxide samples prepared at different temperatures.

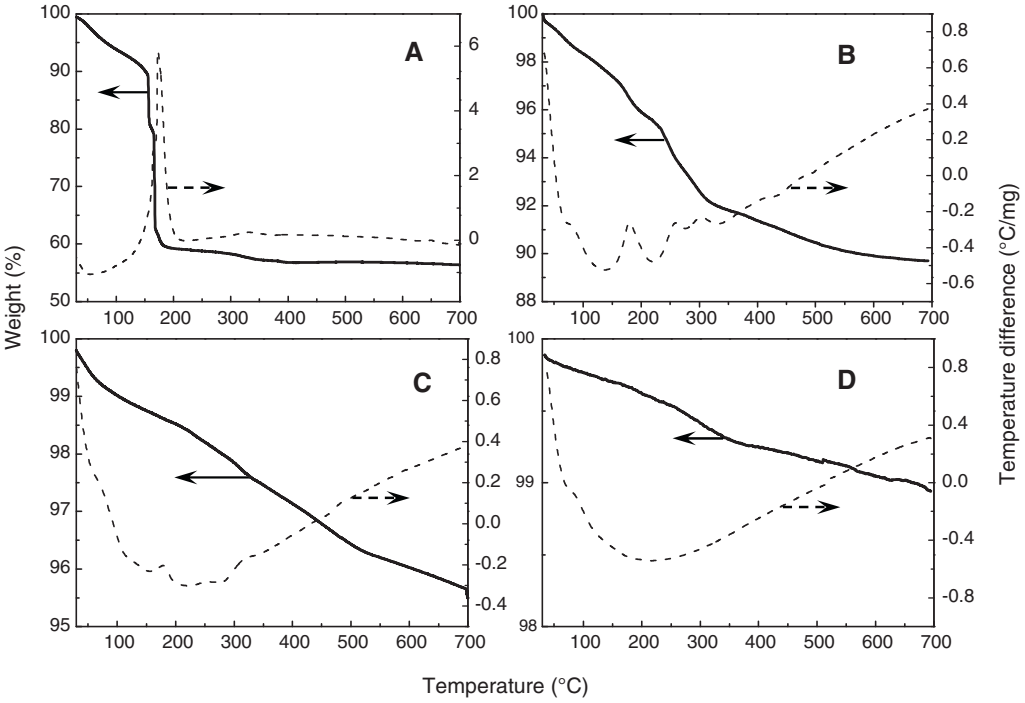

Fig. 6. TG analysis of RuO_2 (A) R-M-80; (B) R-M-200; (C) R-M-350; and (D) R-M-600 (solid lines: weight, dashed lines: temperature difference).

3.3. O_2 evolution measurement

To measure the evolution of the molecular O_2 generated during the reaction, the chronoamperometric measurements are performed at a particular potential for a specified time. For each catalyst, the potential differs and is chosen according to the stability of the catalyst at that particular potential (Fig. 7). The chronoamperometric measurements have been performed at 1.5 V, 1.6 V and 1.45 V vs. RHE for R-M-200, R-M-350 and R-M-600, respectively, as the surface of the electrode is quite stable at this potential. Fig. 9A–C shows the representative chronoamperograms for R-M-200, R-M-350 and R-M-600, for 60 min, in order to monitor the current decrease until a steady state is achieved.

An integrated apparatus is designed, to quantify gas-volumetric (GV) measurements in the reaction. The accurate weight measurement of water displaced by the oxygen evolved during the course of the reaction is determined. Oxygen bubble adhered to the electrode surface can decrease the available active sites for the reaction and may affect the peak currents. Thus the catalyst is placed in the solution by keeping the working electrode horizontally (catalyst upwards), to reduce the rest of the evolved gas bubble on the surface of the catalyst. As a result of oxygen evolution, the pressure inside the reactor flask increases causing the water flow from spiral tube water reservoir toward the collection chamber, and quantified by the electronic balance until the reaction ends.

The oxidation current by the catalyst R-M-200 initially shows large current values (Fig. 9A). This current density drops exponentially to lower values in few minutes, which shows the instability of the catalyst at the potential employed for long time. Due to the hydrous nature, the Ru–Ru bond may not be strong enough in R-M-200 and thus unstable for long time. In case of R-M-350, initially

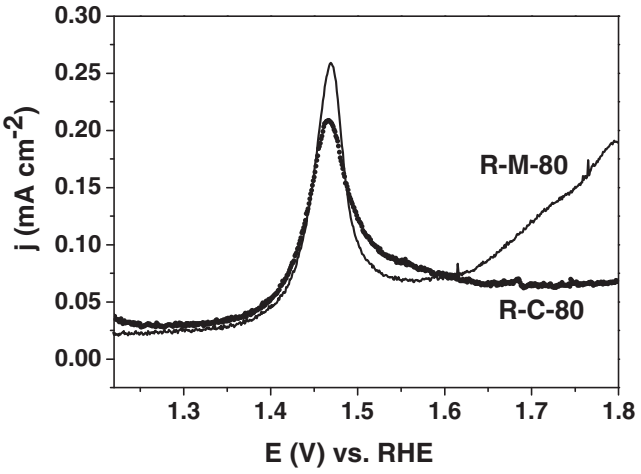

Fig. 7. Polarization curves of RuO_2 for Oxygen evolution reaction in 0.5 M H_2SO_4 at a scan rate $\nu = 10$ mV s^{-1} and $T = 25$ °C.

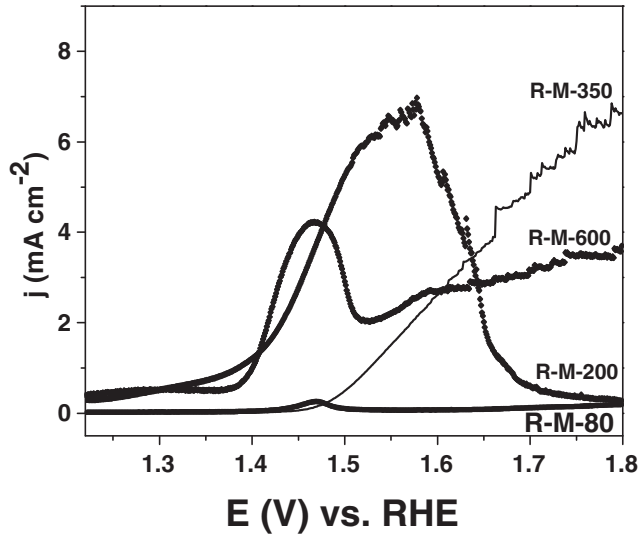

Fig. 8. Polarization curves of RuO_2 samples annealed at different temperatures for oxygen evolution reaction in 0.5 M H_2SO_4 at a scan rate $\nu = 10$ mV s^{-1} and at $T = 25$ °C.

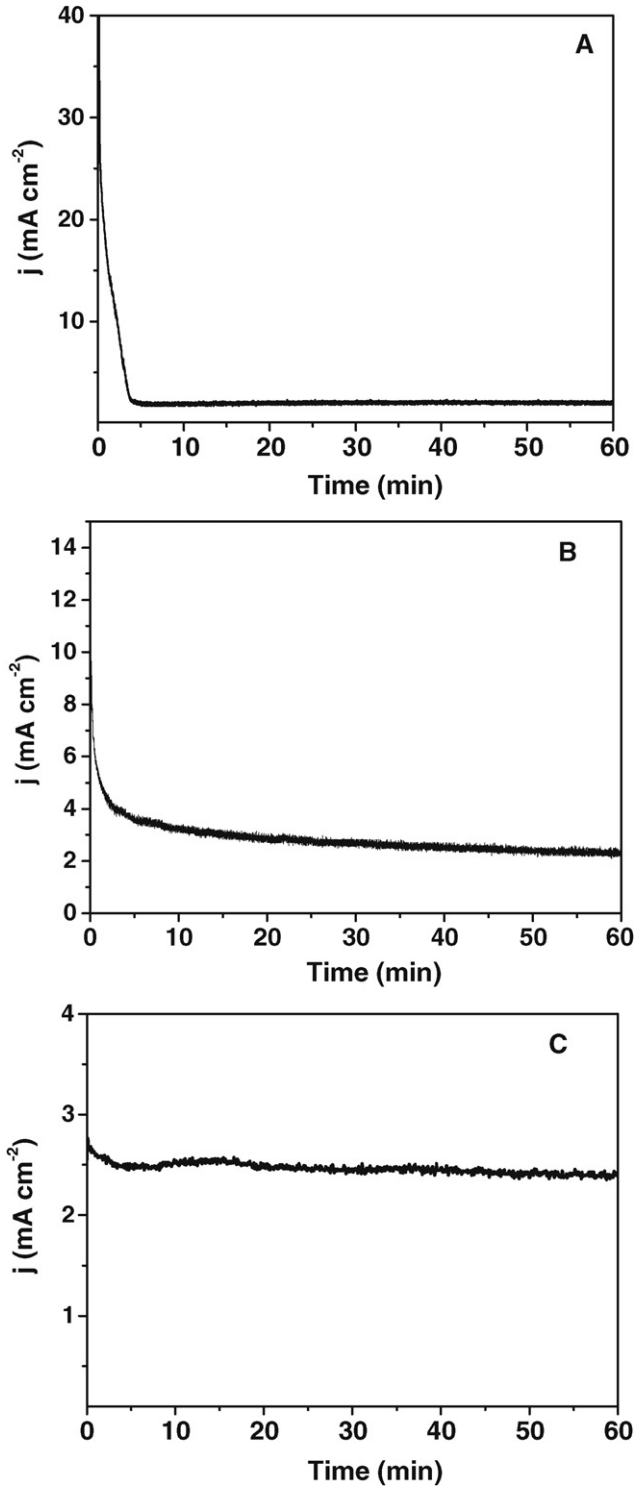

Fig. 9. Anodic current density recorded in course of oxygen evolution measurement in 0.5 M H_2SO_4 solution by (A) R-M-200 at 1.5 V vs. RHE; (B) R-M-350 at 1.6 V vs. RHE; and (C) R-M-600 at 1.45 V vs. RHE (T = 25 °C).

the current drop is observed, but stabilizes to a constant current value (ca. 3 mA cm^{-2}) after a short time. Fig. 9B shows the stable current density at the applied voltage 1.6 V vs. RHE, for the period of time monitored. R-M-600 catalyst exhibited less current density at 1.45 V vs. RHE (Fig. 9C). The observed current value is found to be stable for the period of time. The higher synthesis temperature of R-M-600 caused the sintering and crystallisation of the material, thus leading to decrease in the surface area, loss of the hydration of the ruthenium oxide compound and poor proton conductivity, which resulted to yield low current density. For the continuous evolution of oxygen, when the catalyst employed in PEM electrolysers, it is important to have a good stability over the range of potentials applied for a long time. But the successive cyclic voltammograms in the potential range between 1.1 V and 1.8 V vs. RHE, and 0.9 V and 1.5 V vs. RHE, illustrated the non regenerative active surface for R-M-200 and R-M-600 catalysts (Figs. SI1 and SI2, supporting information). Therefore neither too low nor too high annealing temperatures of the catalyst are best suited for this application. Thus the optimum temperature to synthesise the catalyst for the evolution of oxygen is found to be 350 °C by the present method. The mechanism of oxygen evolution by metal oxide involves the discharge of the water molecules at the surface to form adsorbed hydroxyl radicals. This adsorbed hydroxyl radicals are electrochemically oxidized to oxygen or to higher oxide state of the metal, which decompose to yield oxygen. The presence of more active sites on the surface of the metal oxide for the adsorption of hydroxyl radicals determines the better performance of the catalyst toward the anodic oxygen evolution reaction. The annealing temperature for the preparation of R-M-350 favoured the uniform distribution of particles with better physical and chemical stability toward O_2 evolution at 1.6 V.

The amount of evolved oxygen by the metal oxide R-M-350 during electrolysis was compared to the measurement of the faradic charge at constant voltage estimated by integrating the area of the chronoamperogram (Fig. 9B). The current integration at 1.6 V for 60 min is found to be ca. 18 C. As the oxygen evolution is a four electron process, the number of moles for this process is found to be almost equal to 4.6×10^{-5} mol. The amount of oxygen simultaneously recovered was 1.2 mL, which corresponds to 5.04×10^{-5} mol. This result indicates that the whole faradic charge was employed for the generation of oxygen.

3.4. Supercapacitive property studies

It is noteworthy that at low temperatures, the amorphous phase is acquired which is normally less stable at higher energies. This amorphous or hydrous RuO_2 is feasible for supercapacitor application, since the protons can easily permeate through the bulk of the amorphous RuO_2 electrode and whole amount of electrode is utilized for energy storage.

The practical potential window is set from 0.3 V to 1.2 V vs. RHE in 0.5 M H_2SO_4, to avoid the faradic process. For the specific capacitance measurements, 0.0136 mg of the material is deposited on the polished glassy carbon electrode. The capacitance of the material is determined by calculating the average of the charge and discharge current values. The specific capacitance (C) of the material is determined by Eq. (2):

$$C = \frac{I}{(dE/dt) \times m} \quad (2)$$

where I is the average of charge–discharge current in amperes (dE/dt) is the scan rate in mV s^{-1} and m is the mass in mg of the active material deposited on the working electrode. In aqueous acid electrolytes, the fundamental charge storage process is proton insertion into the bulk material.

Fig. 10 shows the cyclic voltammograms (CV) of the ruthenium oxide electrodes measured as a function of the potential scan rate in 0.5 M H_2SO_4 solution. The potential scan rate was varied from 5 mV s^{-1} to 50 mV s^{-1}, in order to evaluate the high-rate capability of the ruthenium oxide in the selected potential window. The specific capacitances for the RuO_2 materials annealed at different temperatures are determined and illustrated in Table 1. The general shape of the CVs remains unchanged with the scan rate, which shows that the *iR* loss is insignificant within the scan rate range

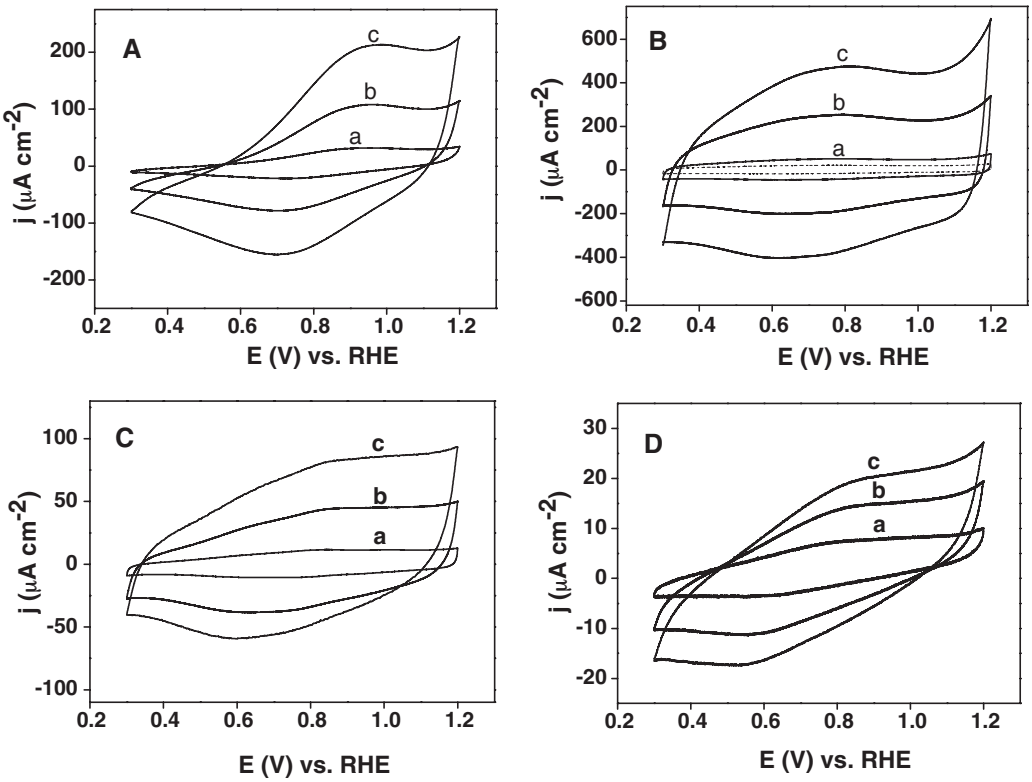

Fig. 10. Cyclic voltammograms recorded at different scan rates (a = 5 mV s^{-1}; b = 25 mV s^{-1}; c = 50 mV s^{-1}; dotted lines = 2 mV s^{-1}), in 0.5 M H_2SO_4 solution for the catalyst (A) R-M-80; (B) R-M-200; (C) R-M-350; and (D) R-M-600.

studied. All CV curves are almost symmetrical to zero potential line. The hydrous R-M-80 demonstrates the specific capacitance of 396 F g^{-1} at the scan rate of 5 mV s^{-1} (Fig. 10A). When the scan rate is increased to 25 mV s^{-1} and 50 mV s^{-1}, the specific capacitance decreased to 275 F g^{-1} and 270 F g^{-1}, respectively.

In Fig. 10B, the material R-M-200 (hydrous and partially crystalline ruthenium oxide) shows rectangular shaped cyclic voltammograms at all potential scan rates with a steep change in the current flow direction at each limit of the potential window. The specific capacitance for this hydrous RuO_2 (R-M-200), reaches the maximum value of 716 F g^{-1} at 5 mV s^{-1}. The anhydrous ruthenium oxide film was demonstrated as an ideal capacitor by Galizzioli et al. [30]. The amorphous and hydrous ruthenium oxide formed by the sol–gel method found to have the specific capacitance of 768 F g^{-1} [7] at the scan rate of 2 mV s^{-1}, whereas in the thin film formed by electrochemical deposition on titanium substrate, it was observed to be the maximum of 788 F g^{-1}, at the scan rate of 10 mV s^{-1} [31]. These values are comparable with the results obtained by this microwave assisted "Instant method", as the synthesis facilitates the specific capacitance of 737 F g^{-1} at the scan rate of 2 mV s^{-1} for R-M-200, shown in Fig. 10B as dotted lines. Further experiments are carried out by changing the sweep rate on the R-M-200 sample. When the scan rate increased to 25 mV s^{-1} and 50 mV s^{-1}, the specific capacitance decreased to 667 F g^{-1} and 648 F g^{-1}, respectively. At lower sweep rates, the proton gets more amount of time to access the bulk of the oxide. Hence, the specific capacitance increases with decrease in scan rate.

Table 1
Specific capacitance measured at different scan rates in 0.5 M H_2SO_4 of RuO_2 materials annealed at different temperatures from 80 °C to 600 °C.

Scan rate (mV s^{-1})	Specific capacitance (F g^{-1})		
	5	25	50
R-M-80	396	275	270
R-M-200	716	667	648
R-M-350	183	145	133
R-M-600	88	40	29

The change in the magnitude of the current value is observed with different annealed temperatures. Sato et al. observed the influence of capacitance with the oxidation temperature on RuO_2 composites [32]. The specific capacitance of RuO_2 R-M-350 shows the maximum value of 183 F g^{-1} at 5 mV s^{-1}, and it further decrease to 145 F g^{-1} and 133 F g^{-1}, when the scan rate increases to 25 mV s^{-1} and 50 mV s^{-1} respectively. The charge and discharge currents decrease with increase in treatment temperature. As the annealing temperature of the ruthenium oxide material is further increased, the specific capacitance of R-M-600 drastically decreased to 88 F g^{-1}, 40 F g^{-1} and 29 F g^{-1} at the scan rate of 5 mV s^{-1}, 25 mV s^{-1} and 50 mV s^{-1}, respectively. Subramanian et al. [33] observed the specific capacitance for the crystalline RuO_2 by Non-ionic surfactant templating method, and found a value of 58 F g^{-1} at the scan rate of 2 mV s^{-1}.

In the potential range from 0.3 V to 1.2 V vs. RHE, the energy storage behavior can be attributed to the non-faradaic reversible process called the Double-layer capacitance, as the CVs are stable for the subsequent cycles in this potential window. In the double layer field, Juodkazis et al. [34] proposed that the formation of ion-pair was envisaged during charging and discharging process, following Eq. (3).

$$RuO_2{\cdot}H_2O \leftrightarrow RuO_2{}^{+}{\cdot}(OH^-)_{ads} + H^+ + e_{(CB)}{}^- \quad (3)$$

where RuO_2^+ and $e^-_{(CB)}$ represent holes and electrons in valence and conduction bands, respectively. The double layer current capacitance in the potential region between 0.6 and 1.2 V ascribed to reversible adsorption/desorption of OH^- ions on the surface of

RuO_2 phase. Thus the adsorption of anions at 0.6 V in the anodic scan and adsorption of cations in the cathodic scan at 0.8 V was reported by Sugimoto et al. [35].

It was studied in hydrous ruthenium oxide, that the low porosity causes depletion of the electrolyte adsorbed and decrease in power density during charge/discharge measurement [36,37]. Eventhough the compound R-M-80 is more hydrous than R-M-200 (Fig. 2A), the ratio of RuO_2 to H_2O in R-M-80 is comparably lower and thus may also lower the specific capacitance of R-M-80 compared with R-M-200. Zheng et al. [7] explained that for the proton transport, the activation energy was low when the ruthenium oxide material was annealed at critical temperature and the maximum specific capacitance was always obtained at a temperature close to the phase transition from amorphous to crystalline material. It is well agreed with our experimental results that R-M-200 has the maximum specific capacitance, as the commencement of the amorphous to crystalline phase transition is observed at this temperature.

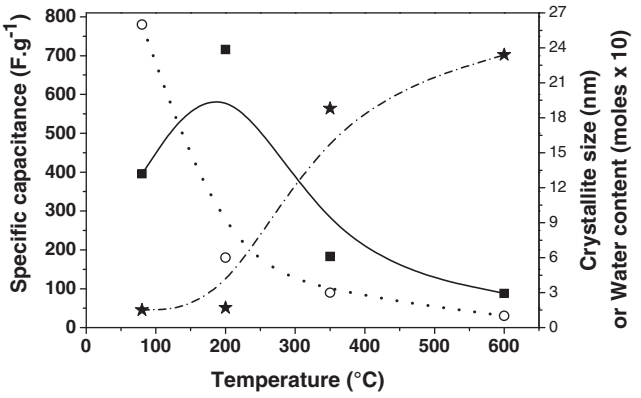

Fig. 11. Specific capacitance (■), crystallite size (℘) and number of water molecules per RuO_2 molecule (○) specific capacitance of various $RuO_2{\cdot}xH_2O$ as a function of annealing temperature.

3.5. Structure and activity relationship

The water plays a crucial role for the synthesis of RuO_2 in this "Instant method", as it is the source of oxygen for the effective formation of metal oxide. The addition of Li_2CO_3 facilitates the formation of uniform nanoparticles of RuO_2 by adsorption on the surface of metal oxide and avoids the growth of nanoparticles. Trasatti and Lodi [8] reported that the anhydrous RuO_2 has the rutile structure, which composed of RuO_6 octahedra, having four oxygen ions at 1.984 Å and two axial oxygen ions at 1.942 Å. This study reveals the fact that the electrochemical response is directly related to the crystallinity of the material. The current density for the oxygen evolution reaction declines with increasing crystallinity and specific electrochemical features begin to emerge. When the annealing temperature increases the water content in the hydrous $RuO_2{\cdot}xH_2O$ decreases and this material becomes progressively more ordered; this is evidenced by *in situ* XRD measurements. As the RuO_6 octahedra is three dimensionally ordered, its electronic conductivity found to be increased. In the present study for the anodic oxygen evolution reaction, the well ordered crystalline RuO_2 (R-M-350) establishes better activity and stability. It was reported that the Ru oxidation state is predominantly + IV, which makes the compound extremely electrochemically stable [35]. The larger Ru–Ru distance in hydrous R-M-200 and the loss of active sites on the surface of highly crystalline R-M-600 led to the deprived performance toward anodic oxygen evolution. Thus the better electrochemical activity for OER requires more interconnected RuO_6 octahedra as well as the structural water content as found in R-M-350 ($[RuO_2{\cdot}0.3H_2O]$ $0.08H_2O$).

The hydrous RuO_2 exhibits excellent super capacitor characteristics with high charge density distributed across a wide double layer potential window. According to Zheng and Jow [38], amorphous Ru oxides allow the whole bulk of RuO_2 to be utilized for energy storage due to the fast proton transport rates. The further increase in the oxidation temperature results in utilizing only the surface of the oxide. The proton transport rate is decreased and not all of the bulk oxide is utilized. Maximum capacitance is obtained when both electron and proton transport rates are optimized. Removal of total structural water from RuO_2 (R-M-600) results in lowering the proton transport through the oxide. The lower charge density for the highly crystalline sample (R-M-600) is attributed to the lower hydration and thus becomes surface sensitive with the less participation of the bulk. Hence, at higher current densities mass transfer becomes limiting and the capacitance start decreasing. The specific capacitance of RuO_2 was found to be sensitive to the crystalline structure [7], as the lattice of the material is rigid and is difficult to expand for the insertion of protons. Thus the crystalline nature of the electrode (above 200 °C annealed samples), limits supercapacitor performance through the surface charge transfers reaction.

The mechanism of surface charge generation can be enumerated as: surface dissociation, ion adsorption from solution, and crystal lattice defect. The increase in the current values of the cyclic voltammograms can also be explained in terms of the oxide surface hydration phenomenon. Fig. 11 compares the specific capacitance, the crystallite size and the amount of structural water content as a function of temperature. The specific capacitance markedly differs from hydrous to crystalline and depends on the ability to balance both electron transport along the dioxo bridges and proton transfer through structural water necessary for charge storage. The proton transfer is well balanced by the hydrous RuO_2 (R-M-200) which enhanced the specific capacitance to 737 $F\,g^{-1}$ at a scan rate of 2 $mV\,s^{-1}$. At higher temperatures, crystalline RuO_2 is obtained but leads to the inhibition of proton insertion resulting in decrease of capacitive current. An optimum mixed percolation conduction mechanism where separate percolation paths provide protonic and electronic conduction has also been proposed [39]. Additionally, when the annealing temperature for R-M-80 increases, the loss of structural water molecules leads to the increase in size of RuO_2 (Fig. 11). For R-M-200, a slight increase of particle size (1.7 nm) is observed from TEM measurement and the value of structural water content is found to be 0.6 mol per RuO_2. Thus it approaches a nominal composition of hydrous RuO_2 which provides a fast proton transfer [7]. The increase in annealing temperature to 350 °C led to drastic increase in average size of RuO_2 nanocrystals to 19 nm with 0.3 mol of structural water molecules for R-M-350, facilitating better electronic conduction [29]. Considering the further increase of heat treatment temperature, it resulted in a large increase in the average size of RuO_2 (up to 23 nm for R-M-600). The increase of the RuO_2 particle size is accompanied by a loss of real surface area of the material. Therefore, the decrease of the capacitance as expressed per unit mass of material for RuO_2 materials annealed at temperature higher than 200 °C could mainly be due to the decrease of the real active surface area, even if the change in structural water content has also to be considered. Thus this study infers that the hydrous regions within the RuO_2 nanoparticles allow facile proton permeation into the bulk material for efficient charge storage while the interconnected RuO_6 octahedra accounts for the electronic conduction. Thus, the tailoring of RuO_2 material - hydrous RuO_2 for super capacitor and crystalline RuO_2 as catalyst for OER, can be made by the present method for the various electrochemical applications.

4. Conclusions

RuO_2 nanoparticles are synthesized by "Instant method" under microwave radiation. The microwave assisted "Instant method" is rapid, cheap and resulting in homogeneous crystalline RuO_2 nanostructures. This method is effective for synthesizing catalysts active toward the OER and also for synthesizing the hydrous RuO_2, which is most viable for supercapacitor applications. This study highlights the feasibility of RuO_2 materials for various applications by a single synthetic route. Simplicity and economic viability makes this synthesis very attractive and also the method is efficient to scale-up to a macro level, which exhibits the same physical and electrochemical properties.

For the anodic oxygen evolution in 0.5 M H_2SO_4, the microwave synthesized RuO_2 catalyst shown increased current density than the catalyst prepared by classical heating method. The characterizations of the sample R-M-80 indicate a chemical composition of $[RuO_2{\cdot}2.6H_2O]$ $0.7H_2O$ (TGA), the formation of uniform nanoparticles of hydrous RuO_2 with an average diameter of 1.5 nm (TEM), an amorphous nature (XRD); but the Raman spectra demonstrated the characteristic spectrum of Rutile type RuO_2. After annealing the as-prepared ruthenium oxide compound at 350 °C (R-M-350), the structural formula is derived as $[RuO_2{\cdot}0.3H_2O]$ $0.08H_2O$ from TGA. The formation of well defined nanostructured RuO_2 crystals in R-M-350 is substantiated by XRD, Raman and TEM analysis. The material R-M-350 acquired to have better stability and electrocatalytic activity toward OER. The quantitative measurement for the oxygen evolution using crystalline R-M-350 appears to be effective and reliable with the electrical energy supplied for the oxygen evolution reaction. However, the hydrous R-M-200 material exhibits the structural formula as $[RuO_2{\cdot}0.6\ H_2O]$ $0.14H_2O$, provides high power capability, excellent reversibility for a wide potential and thus exhibits larger capacitance. The specific capacitance of R-M-200 is found to be 737 F g^{-1} at the scan rate of 2 mV s^{-1} and it decreases with the annealing temperature or crystallinity to 88 F g^{-1} at 5 mV s^{-1} for R-M-600.

Appendix A. Supplementary data

Supplementary data associated with this article can be found, in the online version, at doi:10.1016/j.jpowsour.2010.11.149.

References

[1] S. Trasatti, Electrochim. Acta 45 (2000) 237.
[2] B. Wang, J. Power Sources 152 (2005) 152.
[3] J.-H. Kim, A. Ishihara, S. Mitsushima, N. Kamiya, K.-I. Ota, Electrochim. Acta 52 (2007) 2492.
[4] C.L.P.S. Zanta, A.R. De Andrade, J.F.C. Boodts, Electrochim. Acta 44 (1999) 3333.
[5] L. Nanni, S. Polizzi, A. Benedetti, A. De Batistti, J. Electrochem. Soc. 146 (1999) 220.
[6] T. Liu, W.G. Pell, B.E. Conway, Electrochim. Acta 42 (1997) 3541.
[7] J.P. Zheng, P.J. Cygan, T.R. Jow, J. Electrochem. Soc. 142 (1995) 2699.
[8] S. Trasatti, G. Lodi, in: S. Trasatti (Ed.), Electrodes of Conductive Metal Oxides, Elsevier, Amsterdam, 1981, p. 521, Part B.
[9] E.R. Kotz, S. Stucki, J. Appl. Electrochem. 17 (1997) 1190.
[10] T. Lassati, J. Boodts, L. Bulhoes, J. Non-Cryst. Solids 273 (2000) 129.
[11] E. Rasten, G. Hagen, R. Tunold, Electrochim. Acta 48 (2003) 3945.
[12] R. Adams, R. Shriner, J. Am. Chem. Soc. 45 (1923) 2171.
[13] S.Y. Kang, K.H. Choi, S.K. Lee, C.S. Hwang, H.J. Kim, J. Korean Phys. Soc. 37 (2000) 1040.
[14] J.L. Fernández, M.R. Gennero de Chialvo, A.C. Chialvo, J. Appl. Electrochem. 27 (1997) 1323.
[15] J.H. Yi, P. Thomas, M. Manier, J.P. Mercurio, J. Phys. IV Fr. 8 (1998) 45.
[16] Y.S. Huang, P.C. Liao, Sol. Energy Mater. Sol. C 55 (1998) 179.
[17] M. Hiratani, Y. Matsui, K. Imagawa, S. Kimura, Thin Solid Films 366 (2000) 102.
[18] H. Kim, B.N. Popov, J. Power Sources 104 (2002) 52.
[19] Y. Wang, J.Y. Lee, J. Power Sources 144 (2005) 220.
[20] S. Yan, H. Wang, P. Qu, Y. Zhang, Z. Xiao, Synthetic Met. 159 (2009) 158.
[21] J.-Y. Kim, K.-H. Kim, S.-H. Park, K.-B. Kim, Electrochim. Acta 55 (2010) 8056.
[22] M.T. Reetz, H. Schulenburg, M. Lopez, B. Splienthoff, B. Tesche, Chimia 58 (2004) 896.
[23] M.T. Reetz, M. Lopez, Patent Application DE-A 102 11701.2, 16.03.2002.
[24] H.H. Kim, K.B. Kim, J. Electrochem. Soc. 151 (2004) E7;
D.A. McKeown, P.L. Hagans, L.P.L. Carette, A.E. Russell, K.E. Swider, D.R. Rolison, J. Phys. Chem. B 103 (1999) 4825.
[25] K.H. Chang, C.C. Hu, C.Y. Chou, Chem. Mater. 19 (2007) 2112;
Y.S. Huang, F.H. Pollak, Solid State Commun. 43 (1982) 921.
[26] S. Music, S. Popovic, M. Maljkovic, K. Furic, A. Gajovic, Mater. Lett. 56 (2002) 806;
S. Sarangapani, P. Lessner, J. Forchione, A. Griffith, A.B. Laconti, J. Power Sources 29 (1990) 355.
[27] J.V. Ryan, A.D. Berry, M.L. Anderson, J.W. Long, R.M. Stroud, V.M. Cepak, V.M. Browning, D.R. Rolison, C.I. Merzbacher, Nature 406 (2000) 169.
[28] J.L. Gomez de la Fuente, M.V. Martinez-Huerta, S. Rojas, P. Hernández-Fernández, P. Terreros, J.L.G. Fierro, M.A. Penã, Appl. Catal. B Environ. 88 (2009) 505.
[29] O. Petrii, J. Solid State Electr. 12 (2008) 609.
[30] D. Galizzioli, F. Tantardini, S. Trasatti, J. Appl. Electrochem. 4 (1974) 57.
[31] B.O. Park, C.D. Lokhande, H.S. Park, K.D. Jung, O.S. Joo, J. Power Sources 134 (2004) 148.
[32] Y. Sato, K. Yomogida, T. Nanaumi, K. Kobayakawa, Y. Ohsawa, M. Kawai, Electrochem. Solid State Lett. 3 (2000) 113.
[33] V. Subramanian, S.C. Hall, P.H. Smith, B. Rambabu, Solid State Ionics 175 (2004) 511.
[34] K. Juodkazis, J. Juodkazytė, V. Sukienė, A. Grigucevicienė, A. Selskis, J. Solid State Electrochem. 12 (2008) 1399.
[35] W. Sugimoto, K. Yokoshima, Y. Murakami, Y. Takasu, Electrochim. Acta 52 (2006) 1742.
[36] D.R. Rolison, P.L. Hangans, K.E. Swider, J.W. Long, Langmuir 15 (1999) 774.
[37] T.P. Gujar, V.R. Shinde, C.D. Lokhande, W.-Y. Kim, K.-D. Jung, O.-S. Joo, Electrochem. Commun. 9 (2007) 504.
[38] J.P. Zheng, T.R. Jow, J. Electrochem. Soc. 142 (1995) L6.
[39] W. Dmowski, T. Egami, K.E. Swinder-Lyons, C.T. Love, D.R. Rolison, J. Phys. Chem. B 106 (2002) 12677.